

Acoustical Nonlinearities in Aircraft Flyover Data

Sally M^cInerny¹

The University of Alabama, Tuscaloosa, AL 35487

Kent L. Gee²

Brigham Young University, Provo, UT 84602

Micah Downing³ and Michael James⁴

Blue Ridge Research and Consulting, LLC, Asheville, NC 28801

Numerous analyses techniques have been proposed as means of characterizing acoustical nonlinearities in high-thrust engine noise. These include probability distributions for the pressure and the time derivative of the pressure (i.e., the gradient), the skewness and kurtosis coefficients of the pressure and its time derivative, and Howell-Morfey nonlinear indicators. In this paper, a number of these analyses techniques are applied to acoustic data recorded during a series of military jet flyovers. The analysis examines these different measures as a function of microphone height above the ground. This analysis provides strong indications that microphone should be mounted well above the ground to properly measure nonlinearities in high-thrust engine noise.

Nomenclature

f	=	Frequency, Hz
F	=	Engine thrust, N
$FT\{\}$	=	Fourier transform operator
K	=	kurtosis coefficient
$P_{rms}(f)$	=	Constant bandwidth rms pressure spectrum
S	=	Skewness coefficient
SPL	=	Sound pressure level, dB re 20e-6 Pa
S/R	=	Source to receiver distance, m
T	=	Time in Greenwich Mean Time
U_e	=	Mean exhaust velocity at nozzle exit plane, m/s;
*	=	complex conjugation operator

I. Introduction

RECENT studies have concluded that nonlinear effects can play a role in the propagation of noise produced by high-speed jets. These studies have included laboratory model-scale studies¹⁻³, numerical simulations⁴⁻⁵, and experimental studies on full-scale military jet aircraft.⁶⁻⁸ Exhaust noise of sufficient intensity so as to produce nonlinear propagation is caused by supersonic exhaust velocities that result in relatively efficient and directional Mach wave radiation. These Mach waves can be highly skewed, meaning that the positive (compressive) pressure fluctuations are greater in amplitude than the rarefactions (e.g., Ref. 9). The intense compressive portions of the waveform will be more likely to propagate nonlinearly than the portions of the noise signature that are lower in amplitude.

Two inter-related factors act to increase the propensity for steepened waveforms at the source as well as further nonlinear propagation effects. Increases in engine thrust are generally achieved by increasing exhaust velocities, as

¹ Assoc. Prof., Dept. of Aerospace Engineering and Mechanics, P.O. Box 870280, Tuscaloosa, AL 35487, member.

² Assist. Prof., Dept. of Physics and Astronomy, N319 ESC, Provo, UT 84602, member AIAA.

³ Chief Scientist, Blue Ridge Research and Consulting, LLC, 13 1/2 W. Walnut St., Asheville, NC

⁴ Principal Engineer, Blue Ridge Research and Consulting, LLC, 13 1/2 W. Walnut St., Asheville, NC

increasing engine size and mass flux may be impractical. These high temperature exhausts have velocities well in excess of the speed of sound in the atmosphere, resulting in Mach wave radiation over a considerable portion of the exhaust plume.^{10,11} As the engine mechanical power increases, so does the acoustic efficiency.¹²⁻¹⁴ The combination of increased thrust (for a fixed exhaust diameter) and therefore increased mechanical power, coupled with increased radiation efficiency results in sound levels that promote greater nonlinear propagation effects.

Nonlinear propagation effects, which are characterized by waveform steepening and possible shock formation and coalescence in the time domain and spectral broadening in the frequency domain, are an issue for at least two reasons. First, the unique characteristics of nonlinearly propagated noise have been shown to be significant from a human perception standpoint, despite the fact that conventional noise metric calculations are very similar for nonlinearly and linearly propagated signals.¹⁵ Furthermore, analysis of time waveform data for the purposes of aircraft identification and location can be complicated by the significant changes that occur due to nonlinearity.

There have been multiple analyses of military aircraft flyover noise (e.g., Refs. 16 and 17), but only one that has analyzed flyover noise from a nonlinear propagation perspective. In a preliminary study, McNerny *et al.*⁸ analyzed several flyover runs of a jet aircraft at different engine power and flight conditions. They found that, on average, there was not a strong correlation between the skewness coefficient of the acoustic pressure waveform and overall sound pressure level. They did conclude, however, that there was a strong correlation between the skewness coefficient of the time gradient of the acoustic pressure and the overall level, suggesting that as level increased, so did the steepness of the time waveforms.

There a number of different variables not accounted for in the previous study by McNerny *et al.*, such as aircraft altitude and the height of microphone off the ground. This latter issue is believed to be of particular significance because data collected at microphones located near the ground are subjected to strong multipath interference effects. These interference effects can have an impact on spectral and statistical estimates of the noise, as well as conclusions regarding the nonlinearity of the propagation.

The purpose of this paper is to present analyses on a limited subset of data acquired during the flyover tests previously reported on by McNerny *et al.* The emphasis is an examination of the signals simultaneously recorded at microphones from 0 to 39 ft off the ground for the same flyover. This paper sheds new insight into the desired location of microphones in order to produce the cleanest measurement results. Because nonlinear propagation effects are expected to be the greatest for military jets operating at afterburner power, two afterburner (AB) flyovers are analyzed in this paper. For these two runs, the influence of microphone height on metrics that are used to characterize nonlinearity in high intensity jet noise is examined.

II. Background of Metrics Used

The theoretical backgrounds behind the techniques used for the flyover data analysis are briefly reviewed. These metrics are important to the full characterization of the noise for a given propagation environment and their calculation for different microphone heights should result in conclusions regarding appropriate microphone placement for flyover tests where large-bandwidth, high-fidelity measurements are desired.

A. One-third Octave Spectra

Constant bandwidth spectra of noise signals with significant shock content exhibit a f^{-2} (6 dB/octave) roll-off at high frequencies.¹⁸ This translates to a 3 dB/octave roll-off for one-third octave spectra. As the noise waveform continues to propagate, however, geometrical spreading and atmospheric absorption result in an exponential decay rate above some characteristic frequency. This characteristic frequency corresponds to the inverse characteristic rise time of the shocks in the waveform.¹⁹ As atmospheric losses cause the shock fronts to gradually thicken during propagation, the characteristic frequency at which the 3-dB/octave roll-off transitions to an exponential roll-off will decrease. However, for frequencies between the peak frequency region and this characteristic frequency, the 3-dB/octave roll-off will continue to hold.

B. Single Number Metrics

Next, a tabularized comparison of simple single number metrics for the analysis period is presented. These metrics include:

- Maximum 0.5 s linearly averaged overall sound pressure level (OASPL)
- L_{eq} for the analysis period
- Skewness coefficient of the pressure

- Skewness coefficient of the pressure time gradient
- Kurtosis coefficient of the pressure
- Kurtosis coefficient of the pressure time gradient

The maximum OASPL is a short time-average indication of the loudest level occurring during a transient event, whereas L_{eq} provides an estimate of the “average” noise level encountered during the event (i.e., within 6 to 10 dB of the maximum). The remaining statistical metrics, which have seen use in the characterization of high-amplitude jet and rocket noise in various studies (e.g., see Refs. 8, 9, 20-23), quantitatively describe the asymmetry (skewness) and relative peakedness (kurtosis) of the probability distributions of the data. Again, the point of this and the remaining analyses is to examine the consistency between the calculated metrics (and, therefore, the data) for a given flyover event as a function of microphone height.

C. Histogram Analyses

Although the skewness and kurtosis coefficients are useful as indicators of non-Gaussian and possible nonlinear behavior, individual moments do not uniquely describe a probability density function. Consequently, an analysis of the data distribution in histogram form and comparison of the histograms as a function of height can be useful. In order to remove differences in OASPL (which translates into differences in the variance), histograms of $p(t)$ will be normalized by the standard deviation of the waveform. This allows the characteristics of the histograms to be viewed on a more consistent basis.

For a sinusoidal signal of rms pressure P_{rms} , the rms value of the time gradient is $2\pi f P_{rms}$. A random noise distribution can, therefore, be expected to have an rms gradient on the order of the peak frequency in the frequency-weighted rms amplitude spectrum, i.e. $f P_{rms}(f)$. Third octave band spectra are frequency weighted by virtue of constant percentage bandwidths, so for a characteristic frequency we used the peak frequency in the 3rd octave band spectra. Based on the spectra measured at 39 feet off the ground, this is about 200 Hz. Thus, the time gradient, $\partial p / \partial t$ was normalized by $2\pi 200 * P_{rms}$, where P_{rms} was the rms value of the pressure during the analysis period. The gradient was calculated using a forward difference with a time step of $1/f_s$, where $f_s=96$ kHz was the sample rate. So, the gradient normalization can be written:

$$\frac{p(t + \Delta t) - p(t)}{\Delta t} \frac{1}{2\pi 200 * P_{rms}} = \frac{\Delta p}{P_{rms}} \frac{f_s}{2\pi 200} \quad (1)$$

D. Time Pressure Gradient versus Pressure Rise

Another analysis to be performed stems from previous work that characterized the steepness of shock fronts of rocket noise²² and of sonic booms.²⁴ One way this can be accomplished is by first calculating the pressure rise in a given shock as

$$\Delta p = p_{\max} - p_{\min} = p(j) - p(i), \quad (2)$$

where i and j respectively represent the time indices of the minimum and maximum pressure, respectively. Next, the maximum value of the time derivative of the pressure between the i th and j th values is estimated using a simple forward difference with sampling interval Δt , yielding

$$\frac{\partial p}{\partial t} \approx \frac{1}{\Delta t} \max\{p(k+1) - p(k)\}, \quad i \leq k < j. \quad (3)$$

The maximum time rate of increase (Eq. (2)) versus pressure rise (Eq. (3)) for a given shock can then be plotted for all of the pressure rise portions of the waveforms. If shocks are present in the data, the slope of the plot at large values of Δp will take on a pressure-squared dependence. The slope of this pressure-squared curve depend on the dominant absorptive mechanisms that control the characteristic rise time of the shocks.²⁵ A full discussion of these plots is provided in Ref. 22.

E. Q/S Plots

The final analysis type has its roots in the efforts of Morfey and Howell²⁶, who developed an ensemble-averaged version of the generalized Burgers equation for the power spectral density, $S_{pp}(f)$. They found that the nonlinear term in the equation was a scaled version of $Q_{p^2_p}(f)$, which is the imaginary part of the cross spectral density (also

called the quadspectral density) of the square of the acoustic pressure and the acoustic pressure. This cross spectral quantity is calculated as

$$Q_{p^2 p}(f) = \text{Im} \left[FT \{ p^2(t) \} FT^* \{ p(t) \} \right]. \quad (4)$$

When Morfey and Howell cast their equation in a dimensionless form, they obtained an indicator of nonlinearity (also dimensionless), expressed as

$$Q/S = \frac{Q_{p^2 p}}{P_{rms} S_{pp}}. \quad (5)$$

The quantity Q/S is an indicator of the net power flux from a given frequency bin. Where the quantity is positive, those frequencies are losing energy due to nonlinearity. If the quantity is negative, the net flux is negative, meaning that those frequencies are gaining energy. The indicator, Q/S , and other quantities that utilize $Q_{p^2 p}(f)$ have been used to examine jet and rocket noise for evidence of nonlinear propagation in a number of recent studies.^{3,27,28,22,2,3,6}

III. Measurements

A. Instrumentation and Measurement Layout

The acoustic measurements used in this analysis were supplemental to an environmental noise data collection effort conducted at Edwards Air Force Base. The flight test consisted of controlled flyovers of a military fighter aircraft. Flights took place during the morning hours when there were moderate 10 knot winds. The supplemental measurement array consisted of 12 microphones as described in Table 1. The general location of the microphones was underneath the flight track and 1,000 ft from the primary array. One set of microphones, #01-#05, were mounted along a 39-ft pole. Microphones #006 and #007 were set on the ground along the flight track and ± 40 feet from the pole. The remaining microphones, #008 - #012, were placed 10 feet from the pole perpendicular to the flight track. Acquisition of the pressure waveforms was carried out using National Instruments 24-bit PXI-4472 DAQ cards with a 96-kHz sampling rate.

Table 1. Microphone Types, Sizes, and Locations.

Microphone			Relative Track Distance	Lateral Offset	Height	Windscreen	Orientation
#	Type	Size	ft	ft	ft		
001	B&K 4939	1/4"	0	0	0	Y	Horizontal
002	B&K 4939	1/4"	0	0	13	Y	Horizontal
003	B&K 4939	1/4"	0	0	26	Y	Horizontal
004	GRAS 40BF	1/4"	0	0	39	Y	Horizontal
005	GRAS 40BF	1/4"	0	0	39	Y	Vertical
006	B&K 4939	1/4"	40	0	0	Y	Horizontal
007	B&K 4190	1/2"	-40	0	0	Y	Horizontal
008	B&K 4939	1/4"	0	-10	5	N	Vertical
009	B&K 4939	1/4"	0	-10	5	N	Vertical
010	GRAS 40BF	1/4"	0	-10	5	N	Vertical
011	B&K 4190	1/2"	0	-10	5	N	Vertical
012	B&K 4190	1/2"	0	-10	0	Y	Horizontal

B. Aircraft Tracking Data

Aircraft tracking data were obtained with onboard systems during the flight test. This data provided spatial location of the aircraft at 0.25-s intervals. The tracking data were time synchronized with the acoustical recordings via an IRIGB time code and translated to the primary array's geometry. This synchronization and translation allows estimation of aircraft distance, flight speed, radiation/ directivity angle (spherical angle measured relative to the exhaust plume), and angle of incidence (relative to the ground plane) as a function of receiver time (see Fig. 1).

For the two AB flyovers (labeled Run 20 and Run 21), the aircraft approached the primary array at low speed at approximately 1,000 ft AGL. When the aircraft reached approximately 1.5 nautical miles before the primary array, afterburner power was selected, and the aircraft performed a climb at an angle of 30 degrees to horizontal in order to minimize acceleration effects. This profile resulted in the aircraft being approximately 2900 ft above the measurement point for Run 20 and 3900 ft for Run 21.

C. Selection of Analysis Period

A running rms pressure calculated using 90% overlap and a linear 0.5 second averaging time was calculated for each microphone and the plots compared. Figure 2 shows the comparison during the peak noisiness time period. The analysis time period was selected so as to encompass levels within 6 to 8 dB of the maximum 0.5s-averaged OASPL. Because levels frequently fell below this bracket and then increased again, there was some subjectivity in the selection period. Given that the purpose here is to compare the results obtained for the same analysis period but using microphones at different heights off of the ground, this does not present a problem. It should be noted, however, that the analysis time period used for the first AB climb recording (Run 20 in the overall set of flights) was 4.9 seconds in duration while that for the second AB climb (Run 21) was only 3.6 seconds in duration. The results obtained for Run 20 are, therefore, more statistically reliable.

For the analysis, the only ground microphone data used were from microphones 6 and 7. These two microphones were placed perpendicular to the flight path directly on the dry lake bed, as is typical for ground measurements at this site. These microphones were located 40 feet to either side (laterally) of the pole microphones and were clear of the pole and tripods, which apparently influenced the data recorded on microphones 1 and 12.

Figure 3 shows the estimated source to receiver distance during the same time period and for the same A/B climb as Fig. 2. For the first A/B climb (Run 20), the source to receiver distance ranged from ~780m to ~1100 m, the directivity angle ranged from ~80 to 44 degrees, and the angle of incidence ranged from ~ 70 through 90° and then back to 75 degrees. For the second A/B climb (Run 21), the source to receiver distance ranged from ~1000m to ~1300 m, the directivity angle ranged from ~80 to 50 degrees, and the angle of incidence ranged from ~ 70 through 90 then back to 80 degrees. Also shown in Fig. 3, top plot, is the ‘corrected’ 0.5-s averaged OASPL. In this case, the minimum source to receiver distance was used as the reference and levels were then corrected for distance, only, to this reference. When these levels are examined as a function of radiation angle (third plot from the top in Fig. 3), one has a better indication of the source directivity.

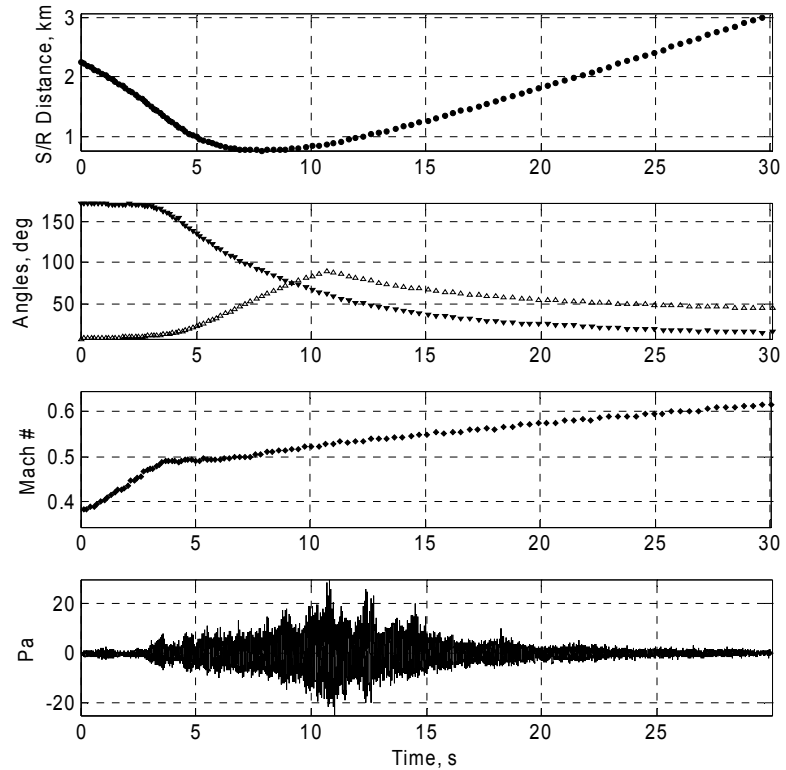


Figure 1. Source to receiver distance, radiation angle and angle of incidence, aircraft Mach number, and sound pressure (Mic. 5) over the recording period during the first A/B climb. The radiation / directivity angle varies from 180 to 0°; the angle of incidence increases from 0° (grazing) to 90° then trails off to just less than 50°.

IV. Analysis Results

A. One-third Octave Spectra Results

Displayed in Figs. 4-6 are the one-third octave spectra for first AB climb (Run 20), represented as bar plots. Run 21 is not shown because of the similarity of the results. In Fig. 4, the 39-ft spectra (black) are compared to ground data. The ground data show an increase in levels at low frequencies relative to the 39-ft spectra due to constructive interference of direct and reflected waves at the ground interface. Note, however, that the increase in level relative to the 39-ft spectra diminishes as the frequency increases. Above the 3.15-kHz one-third octave band, there appears to be a destructive interference pattern.

The 5-ft and 39-ft spectra are compared in Fig. 5. Here, the high-frequency one-third octave bands agree, but there are significant discrepancies in the low and peak-frequency regions of the spectra because of multipath interference effects. Figure 6 shows that these interference effects move to lower frequencies and diminish as the microphone height increases to 13 ft, then 26 ft, then 39 ft. The 39-ft spectra exhibit the smoothest spectral behavior and appear to be free of ground interference effects.

The 39-ft spectrum also reveals information about the shock structure in the propagating waveform. Above the peak frequency of approximately 200 Hz, there is an average 3 dB/octave roll-off up until a frequency of about 1.25 kHz. As discussed before, this roll-off indicates the presence of weak shocks in the data. Above 1.25 kHz, the spectrum transitions to a faster roll off rate that is thought to be controlled by the shock rise times. Neither the 0-ft nor the 5-ft spectra reveal a 3-dB/octave roll-off or the transition in the spectral decay rate. Consequently, microphone height can impact conclusions regarding nonlinearity of the propagation based on one-third octave spectral behavior.

B. Single-Number Metrics

A summary table of calculated metrics for both AB climbs (Run 20 and Run 21) is presented in Table 2. For both runs, the 0.5-s maximum OASPL and the L_{eq} decrease as a function of increasing microphone height between 0 and 13 ft, presumably due to the direct sound and ground-reflected sound exhibiting greater constructive interference closer to the ground. Above 13 ft, however, the levels for each run are consistent to within 0.5 dB. Comparing between the two runs, the near equivalence of the maximum OASPL and the L_{eq} is noted, despite the fact that for Run 21, the aircraft was approximately 20% farther away from the microphones than for Run 20. The cause for the relative increase in level for Run 21 is unknown, but may be attributed to meteorological effects and/or slight differences in engine thrust (the engine conditions for the two runs were nominally the same).

Unlike the level-based metrics, an examination of the statistical calculations does not reveal a clear trend as a function of microphone height. For Run 20, it appears that the pressure data recorded at 5 ft have slightly greater kurtosis coefficients than the other microphone heights. This statistical difference for the 5-ft data is more apparent

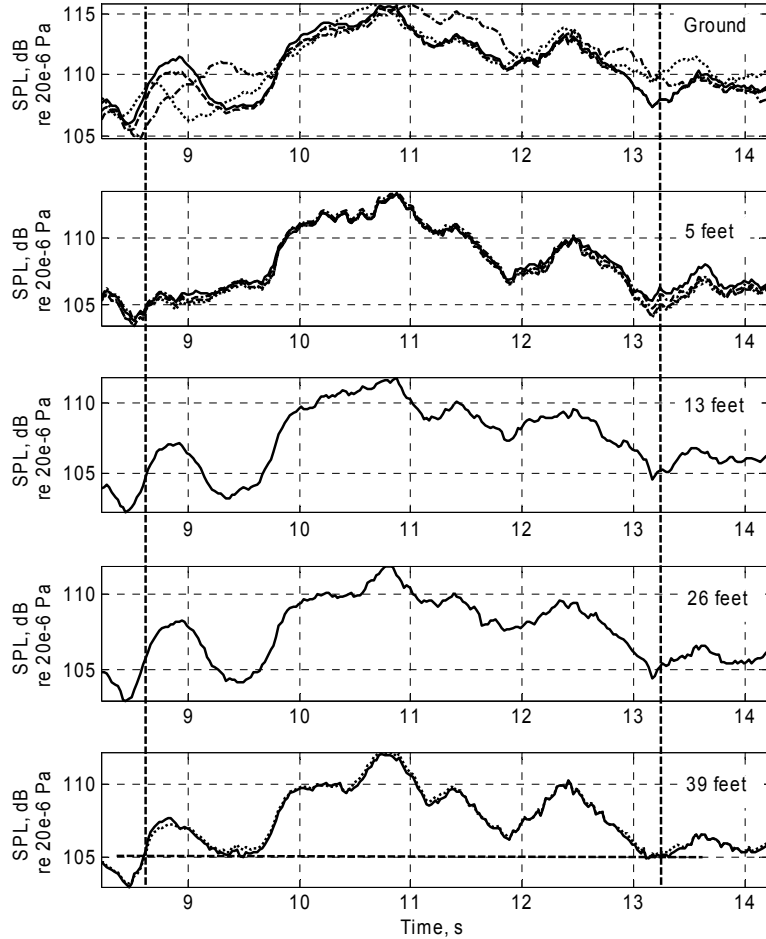


Figure 2. Selection of analysis time period relative to overall SPL of data recorded on ground, at 5 ft, at 13 ft, at 26 ft, and at 39 ft. Selection of the end of the analysis period was subjective; results obtained for different data sets during same period are compared.

in the statistics of $\partial p / \partial t$, where the skewness and kurtosis coefficient values are clearly greater than for the other microphone heights. This trend does not hold for Run 21, though. For Run 21, the skewness and kurtosis coefficients for the pressure are generally greater than Run 20, regardless of microphone height. However, for this run, there is no discernable trend as a function of microphone height in the values of the metrics for the time gradient.

In summary, the tabularized results show that sound pressure levels approach consistent numbers as the microphone height is increased. However, the higher order statistical measures do not follow the same behavior. The statistical moments, by themselves do not appear to be strong indicators of data consistency as a function of microphone height.

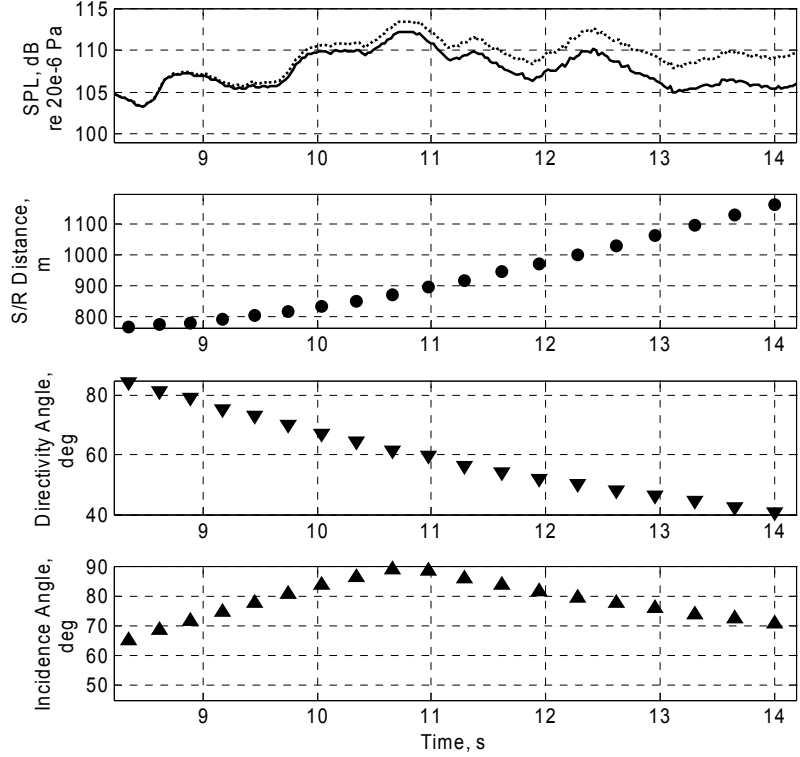


Figure 3. OASPL and adjusted OASPL (see text), source receiver distance, radiation angle, and angle of incidence during period of peak noise levels.

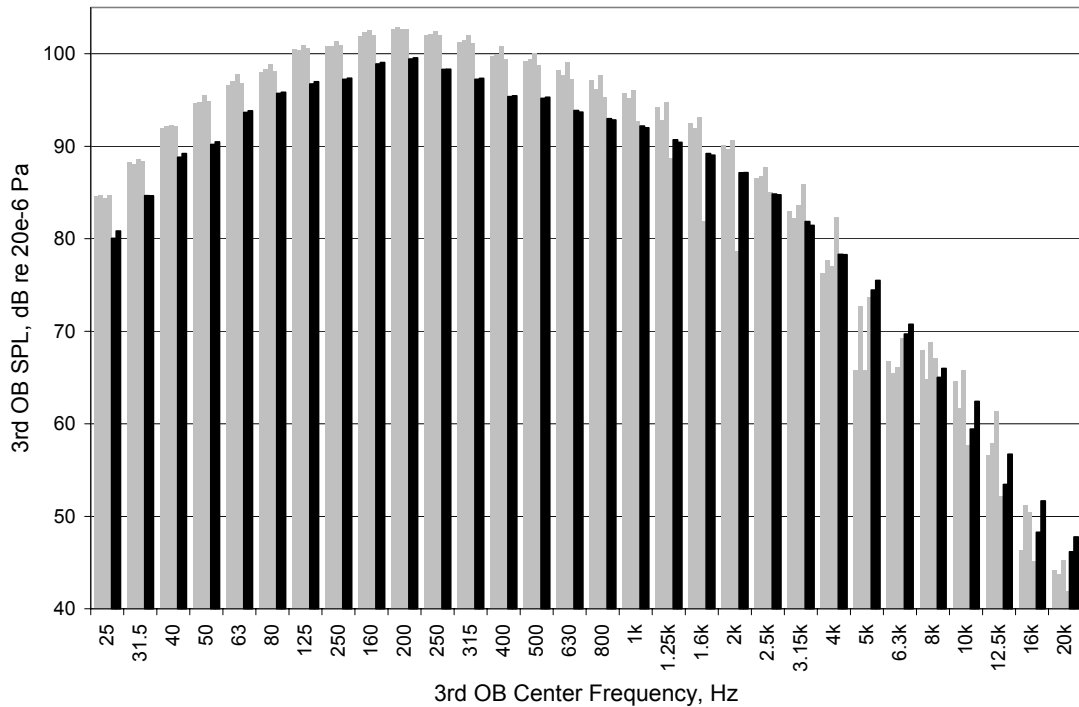


Figure 4. 3rd Octave Band SPLs measured at 39-ft (black bars) and on the ground (gray bars).

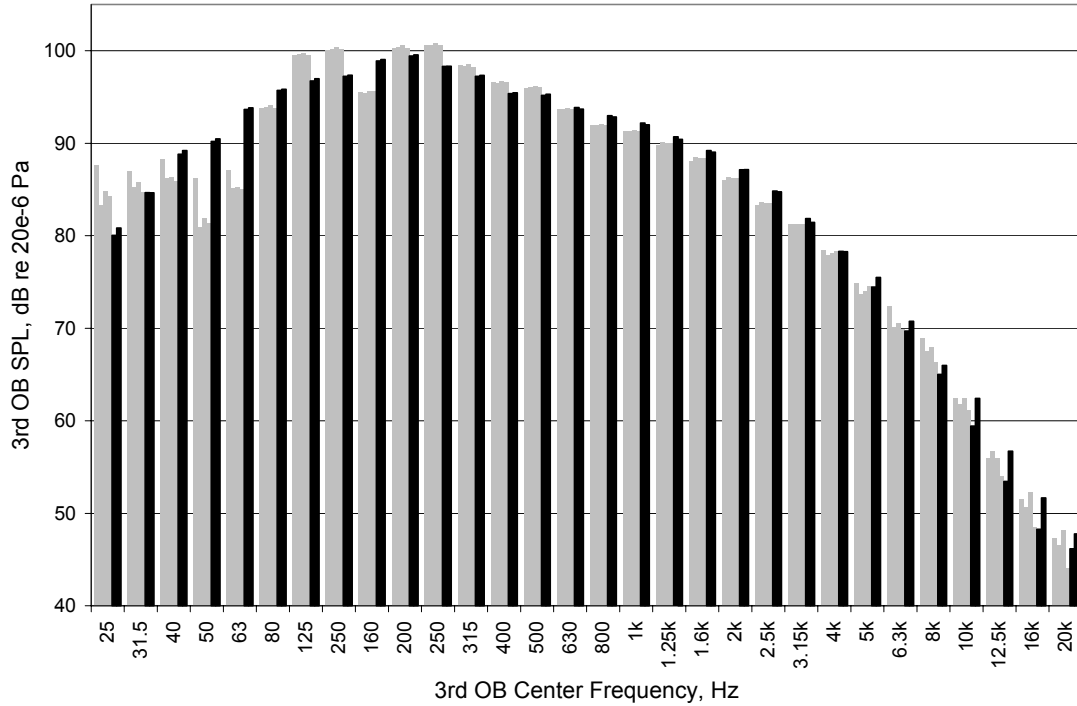


Figure 5. 3rd Octave Band SPLs measured at 39-ft (black bars) and at 5-ft off of the ground (gray bars).

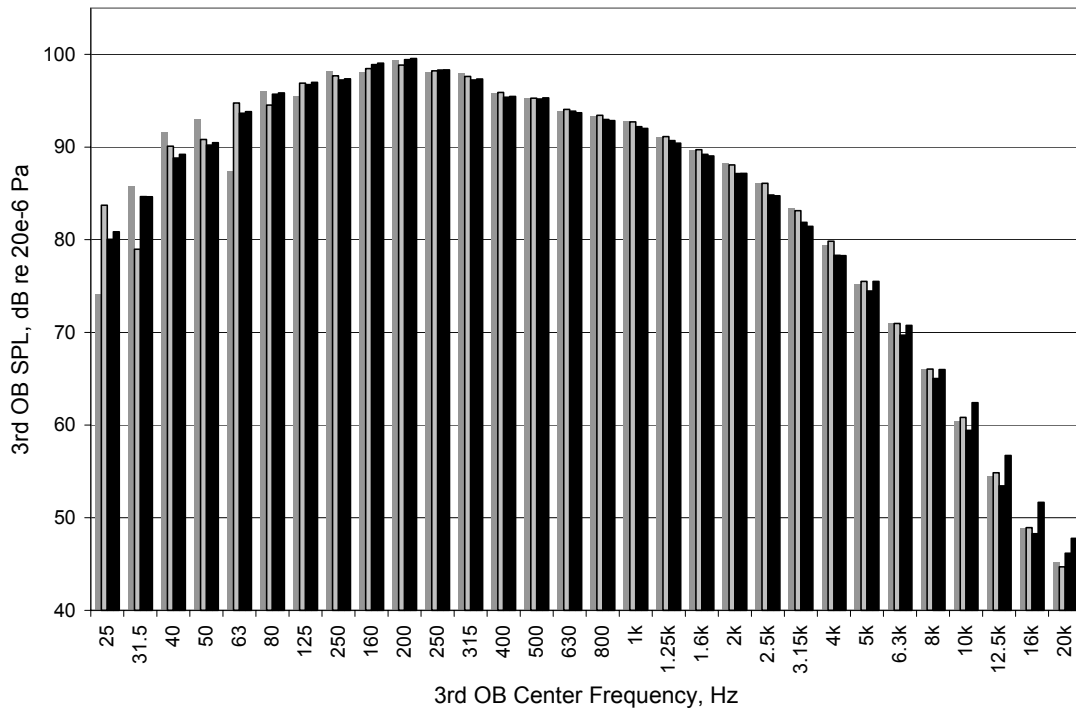


Figure 6. 3rd Octave Band SPLs measured at 39-ft (black bars) , at 13-ft (gray bar), and at 26-ft (darker gray, outline bar).

Table 2. Calculated single number metrics for Runs 20 and 21. For Run 21, the data file for microphone 8 was corrupted and is not included.

Run 20

Ht (ft)	Mic #	Max 0.5 s OASPL	Leq	$S, p(t)$	$K, p(t)$	$S, \partial p / \partial t$	$K, \partial p / \partial t$
0	6	115.4	112.0	0.13	3.7	3.4	28
0	7	115.4	112.5	0.22	3.7	4.3	53
5	8	112.4	109.2	0.07	3.7	5.4	109
5	9	112.4	109.0	0.08	4.0	5.3	105
5	10	112.6	109.3	0.06	3.9	5.3	104
5	11	112.4	109.1	0.07	4.0	5.3	99
13	2	111.4	108.4	0.13	3.7	3.9	42
26	3	111.1	108.5	0.09	3.6	3.8	44
39	4	111.5	108.4	0.05	3.7	3.6	42
39	5	111.7	108.5	0.07	3.7	4.4	67

Run 21

0	6	115.3	111.3	0.27	4.1	3.1	28
0	7	113.1	111.3	0.49	4.6	3.8	47
5	9	113.1	109.1	0.31	4.9	4.5	70
5	10	113.3	109.4	0.29	4.8	4.2	64
5	11	113.1	109.1	0.32	4.9	4.1	60
13	2	112.0	108.8	0.34	4.5	4.5	78
26	3	111.8	108.6	0.30	4.3	5.2	109
39	4	111.5	108.2	0.16	4.1	3.6	48
39	5	111.6	108.4	0.26	4.5	4.0	60

C. Histogram Analysis Results

Single-number statistical moments do not uniquely characterize a probability distribution. Consequently, histogram data for the pressure and its time gradient are shown here for both runs. The acoustic pressure histograms for Runs 20 and 21 are displayed in Fig. 7. The vertical axis is on a logarithmic scale so as to emphasize the characteristics at the tails of the distributions. As discussed in Sec. II, the effect of the different rms levels at different microphone heights has been removed by normalizing each pressure waveform by its standard deviation before calculating the histogram. This normalization yields very similar distributions as a function of microphone height. Note the greater asymmetry in the distributions for Run 21, with positive pressure values occurring out to 6-7 standard deviations. This broad positive tail is the cause for the greater skewness coefficient for $p(t)$ in Run 21 relative to Run 20. These results show that microphone height primarily influences the level (or the variance) of the acoustic pressure waveform, but locating the microphone closer to or farther from the ground does not significantly impact the shape of the pressure distribution.

The histograms for the normalized time gradient of the acoustic pressure are displayed in Fig. 8. The broad positive tails for some of the distributions (e.g., 13 and 26 ft for Run 21) are caused by single occurrences of those gradient values. These results exhibit more variability as a function of microphone height than the pressure data, but, like the skewness and kurtosis coefficients, the trends are fairly inconsistent between Run 20 and Run 21. If it is assumed that the 39-ft data are the most correct representation of the statistics of the pressure time gradient (based on the spectral data), then the major trend that can be pointed out is that locating the microphone closer to the ground can appreciably impact the tails of the time gradient distribution. This feature is noted in Fig. 9, where the ground and 39-ft distributions are directly compared. The 39-ft data show a smooth roll-off in probability from normalized values of 40 to 60, but there is more inconsistency in the ground microphone data in that region of the distribution. However, the results do not show a clear monotonic change in the statistical distribution of the time gradient as the distance between the microphone and the ground decreases. Finally, it is noteworthy that although there were significant differences in the shapes of the pressure histograms for Runs 20 and 21, the histograms of their normalized time gradients are very similar.

D. Shock Plots

The pressure rise versus maximum time gradient results also reveal a disparity between the data at different microphone heights. Displayed in Figs. 10 and 11 are the shock plots for Runs 20 and 21, respectively. A dashed box is shown in each plot to draw attention to the primary region of change between different heights. All plots exhibit the same general behavior. The smaller pressure rises are accompanied by a gradual increase in maximum time gradient. This has been shown by McInerny and Olcmen²² to correspond to the small-signal portions of the waveform where nonlinear steepening is insignificant.

At somewhere between a Δp of 8-20 Pa (as was the case for the rocket noise results in Ref. 22), there is a change in slope. This increase in maximum time gradient at large pressure rises reflects presence of the weak shocks in the data. The gradient for steady weak shocks has been shown to increase as the square of the pressure.^{19,25} As the microphone moves closer to the ground, the weak shock behavior is obscured. That is, for the same pressure rise, the gradient is likely to be smaller.

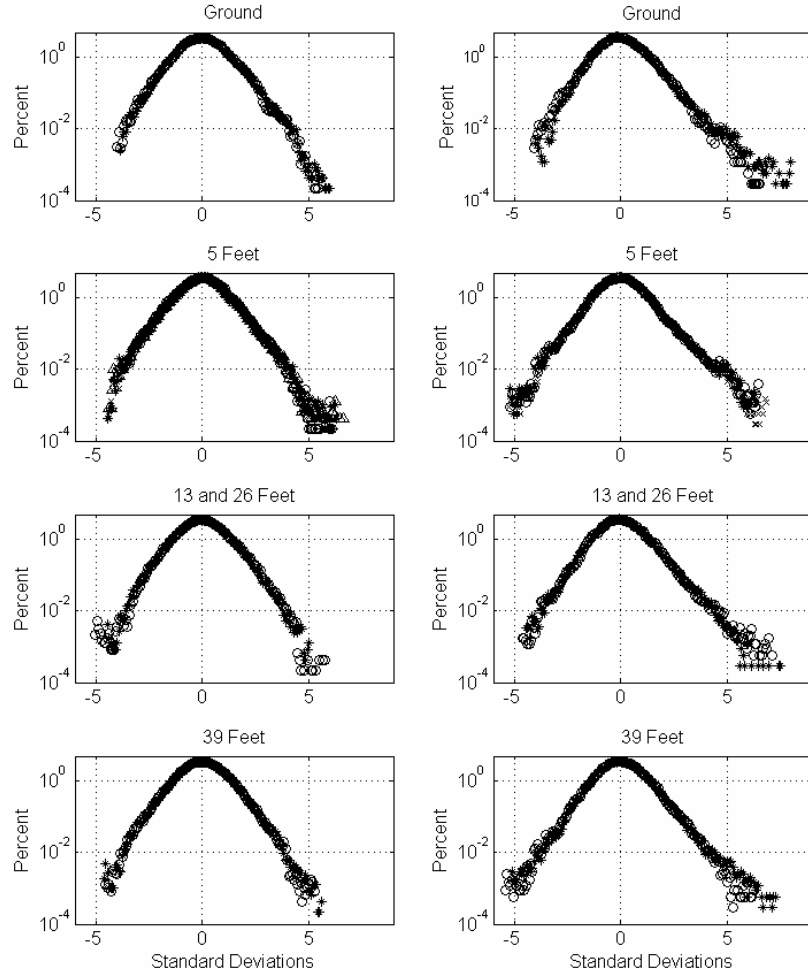


Figure 7. Histograms of normalized acoustic pressure for Run 20 (left) and Run 21 (right), plotted on a log scale to emphasize the behavior of the tails.

E. Q/S Calculations

The plots for Q/S reveal some large differences between the microphone heights for a given run. Before examining these differences, consider the Q/S plots for Mic. 4 (height of 39 ft) for both Run 20 and Run 21 shown in Fig. 12. In these and the subsequent plots shown, Q/S is referred to as the “normalized HM indicator,” where HM denotes Howell and Morfey. The plots in Fig. 12 are consistent with one another; both plots indicate that energy is being lost due to nonlinear interactions at frequencies below 1 kHz and gained at frequencies above 1 kHz. This reflects the expected nonlinear propagation behavior. The fact that the high-frequency energy transfer rapidly approaches zero above 12 kHz is believed to be related not to the physics of the propagation, but to instrumentation noise floor limits. The results for Run 21 are ‘noisier’, which is attributed to there being fewer averages in the calculation since the time series length was shorter (3.6 s versus 4.9 s).

Figure 13 display the Q/S results for a representative microphone at 0, 5, 26, and 39 ft for Run 20. For Run 20, the indicator at 0 and 5 ft are very sensitive to the phase and amplitude changes present at certain frequencies due to ground reflections. At 26 and 39 ft, however, the Q/S calculations are significantly smoother. Finally, Figs. 14 and 15 show the variability of Q/S at fixed microphone heights. Although there are differences in the individual results obtained for different microphones at the same height above the ground, the conclusion regarding the effect of microphone height remains the same. Meaningful and consistent results are obtained for the HM indicator only when the microphones are far enough off of the ground that ground reflections have a negligible effect on the data.

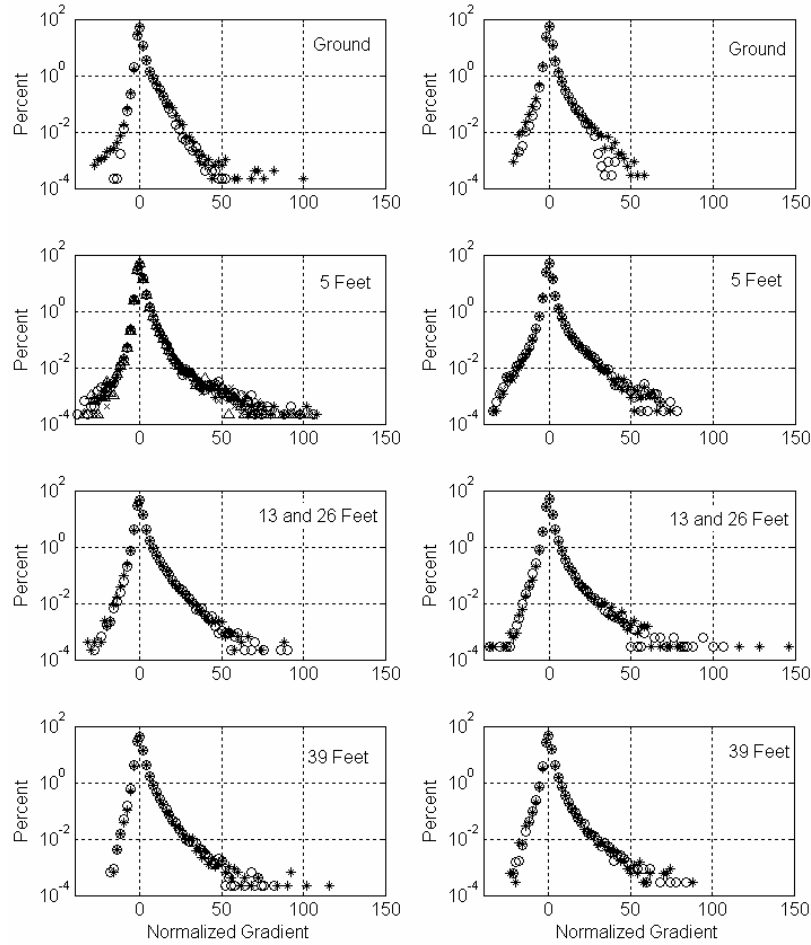


Figure 8. Normalized time gradient (see text for definition) of the acoustic pressure for Run 20 (left) and Run 21 (right).

V. Conclusion

Multiple techniques have been examined as means of characterizing acoustical nonlinearities in high-thrust engine noise data. These techniques include analysis of the acoustic spectra, single valued metrics, histograms of the pressure and pressure gradient, shock plots, and Q/S calculations. These nonlinear indicators have been examined over a range of microphone heights in order to determine the effects of microphone placement on the ability to characterize nonlinearities and to guide proper placement of microphones for future experiments. The analysis shows that cleaner data is obtained with microphones placed higher off the ground. Also, for metrics that characterize nonlinear effects the analysis demonstrates that pressure gradient and Q/S calculations provide the best measures of nonlinear propagation effects.

Acknowledgments

This research was supported in part by the U.S. Department of Defense, through the Strategic Environmental Research and Development Program (SERDP).

References

¹Petitjean, B. P. and McLaughlin, D. K., "Experiments on the Nonlinear Propagation of Noise from Supersonic Jets," AIAA paper no. AIAA-2003-3127, May 2003.

²Petitjean, B. P., Viswanathan, K., and McLaughlin, D. K., "Acoustic Pressure Waveforms Measured in High Speed Jet Noise Experiencing Nonlinear Propagation," AIAA paper no. AIAA-2005-209, Jan. 2005.

³Gee, K. L., Shepherd, M. R., Falco, L. E., Atchley, A. A., Ukeiley, L. S., Jansen, B. J., and Seiner, J. M., "Identification of Nonlinear and Near-field Effects in Jet Noise Using Nonlinearity Indicators," AIAA paper no. AIAA-2007-3653, May 2007.

⁴Wochner, M. S., "Numerical Simulation of Multi-Dimensional Acoustic Propagation in Air Including the Effects of Molecular Relaxation," Ph.D. Thesis, Graduate Program in Acoustics, The Pennsylvania State University, University Park, PA, May 2006.

⁵Brouwer, H. H., "Numerical Simulation of Nonlinear Jet Noise Propagation," AIAA Paper 2005-3088, May 2005.

⁶Gee, K. L., Gabrielson, T. B., Atchley, A. A., Sparrow, V. W., "Preliminary Analysis of Nonlinearity in F/A-18E/F Noise Propagation," *AIAA Journal* Vol. 43, No. 6, 2005, pp. 1398-1401.

⁷Gee, K. L., Sparrow, V. W., James, M. M., Downing, J. M., Hobbs, C. M., Gabrielson, T. B., and Atchley, A. A., "Measurement and Prediction of Noise Propagation from a High-power Jet Aircraft," AIAA paper no. AIAA-2006-2531, May 2006; also submitted to *AIAA Journal* (2006).

⁸McInerny, S., Downing, J. M., Hobbs, C. M., James, M. J., and Hannon, M., "Metrics that Characterize Nonlinearity in Jet Noise," *Innovations in Nonlinear Acoustics: Proceedings of 17th International Symposium on Nonlinear Acoustics*, edited by A. A. Atchley, V. W. Sparrow, and R. M. Keolian, American Institute of Physics Conference Proceedings Series Vol. 838 (AIP, Melville, NY, 2006), pp. 560-563.

⁹Krothapalli, A., Venkatakrishnan, L., and Lourenco, L., "Crackle: A Dominant Component of Supersonic Jet Mixing Noise," AIAA paper no. AIAA-2000-2024, June 2000.

¹⁰McInerny, S.A., "From Jet Noise to Rocket Noise," Proceedings of the 13th Intl. Congress on Sound and Vibration, 2-6 July 2006, Vienna, Austria.

¹¹von Gierke, H.E., "Types of Pressure Fields of Interest in Acoustical Fatigue Problems," WADC Technical Report 59-676, WADC University of Minnesota Conference on Acoustical Fatigue, March 1961.

¹²Dowling, A. P., and Ffowcs-Williams, J.E., *Sound and Sources of Sound*, Halstead Press: a division of John Wiley & Sons, New York, 1983.

¹³Eldred, K., "Prediction of Sonic Exposure Histories," pp. 396-415, *Proceedings FATIGUE of Aircraft Structures*, WADC TR59-507, Wright Air Development Center, 11-13 August, 1959.

¹⁴Guest, S. H., "Acoustic Efficiency Trends for High Thrust Boosters," *NASA TN D-1999*, July 1964, MSFC.

¹⁵Gee, K. L., Swift, S. H., Sparrow, V. W., Plotkin, K. J., and Downing, J. M., "On the Potential Limitations of Conventional Sound Metrics in Quantifying Perception of Nonlinearly Propagated Noise," *Journal of the Acoustical Society of America* Vol. 121, No. 1, 2007, pp. EL1-EL7.

¹⁶Norum, T. D., Garber, D. P., Golub, R. A., Santa Maria, O. L., and Orme, J. S., "Supersonic Jet Exhaust Noise at High Subsonic Flight Speed," NASA/TP-2004-212686, Jan. 2004.

¹⁷Seiner, J.M., Jansen, B.J., and Ukeiley, L.S., "Acoustic Fly-Over Studies of F/A-18 E/F Aircraft During FCLP Mission", AIAA Paper No. 2003-3330, May 2003.

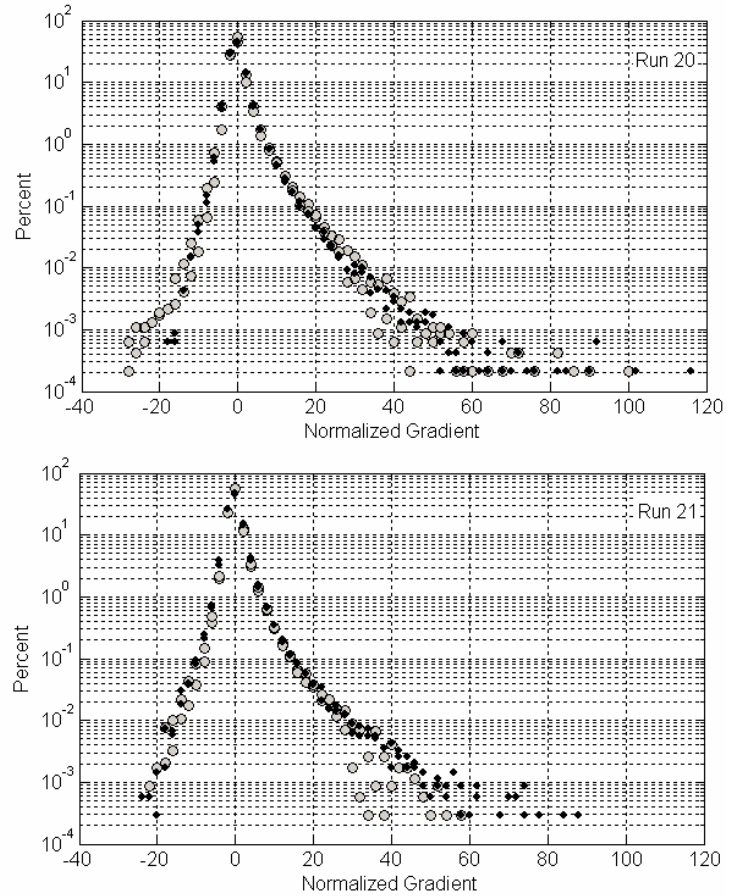


Figure 9. Comparison of normalized time gradient of the acoustic pressure for ground and 39 ft microphones and Run 20 (top) and Run 21 (bottom).

¹⁸Gurbatov, S. N. and Rudenko, O. V., “Statistical Phenomena,” in *Nonlinear Acoustics*, edited by M. F. Hamilton and D. T. Blackstock, Academic Press, San Diego, 1998, Chap. 13.

¹⁹Kang, J. and Pierce, A. D., “Profiles of Fourier Transforms of Weak Shocks Propagating through a Relaxing Atmosphere,” *Proceedings of 3rd IMACS Symposium on Computational Acoustics*, Vol. 2, Elsevier Science Publishers, North-Holland, 1992, pp. 195-207.

²⁰Ffowcs Williams, J. E., Simson, J., and Virchis, V. J., “Crackle: An Annoying Component of Jet Noise,” *Journal of Fluid Mechanics*, Vol. 71, No. 2, 1975, pp. 251-271.

²¹Gee, K. L., V. W. Sparrow, Atchley, A. A., and Gabrielson, T. B., “On the Perception of Crackle in High-Amplitude Jet Noise,” *AIAA Journal*, Vol. 45, No. 3, 2007, pp. 593-598.

²²McInerny, S. A., and S. M. Ölçmen, “High-intensity Rocket Noise: Nonlinear Propagation, Atmospheric Absorption, and Characterization,” *J. Acoust. Soc. Am.*, Vol. 117, No. 2, 2005, pp. 578-591.

²³McInerny, S. A., “Launch Vehicle Acoustics Part 2: Statistics of the Time Domain Data,” *Journal of Aircraft* Vol. 33, No. 3, 1996, pp. 518-523.

²⁴Bass, H. E., Raspet, R., Chambers, J. P., and Kelly, M. “Modification of Sonic Boom Wave Forms During Propagation from the Source to the Ground,” *Journal of the Acoustical Society of America* Vol. 111, No. 1, 2002, pp. 481-486.

²⁵Kang, J. “Nonlinear Acoustic Propagation of Shock Waves through the Atmosphere with Molecular Relaxation,” Ph.D. Thesis, Department of Mechanical Engineering, The Pennsylvania State University (1991).

²⁶Morfe, C. L., and Howell, G. P., “Nonlinear Propagation of Aircraft Noise in the Atmosphere,” *AIAA Journal*, Vol. 19, No. 8, 1981, pp. 986-992.

²⁷Falco, L. E., Atchley, A. A., and Gee, K. L., “Investigation of a Single-Point Nonlinearity Indicator in the Propagation of High-Amplitude Jet Noise,” AIAA paper no. AIAA-2006-2529, May 2006.

²⁸Falco, L. E., “Single-point Nonlinearity Indicators for the Propagation of High-amplitude Acoustic Signals,” Ph.D. Thesis, Graduate Program in Acoustics, The Pennsylvania State University, University Park, PA, May 2007.

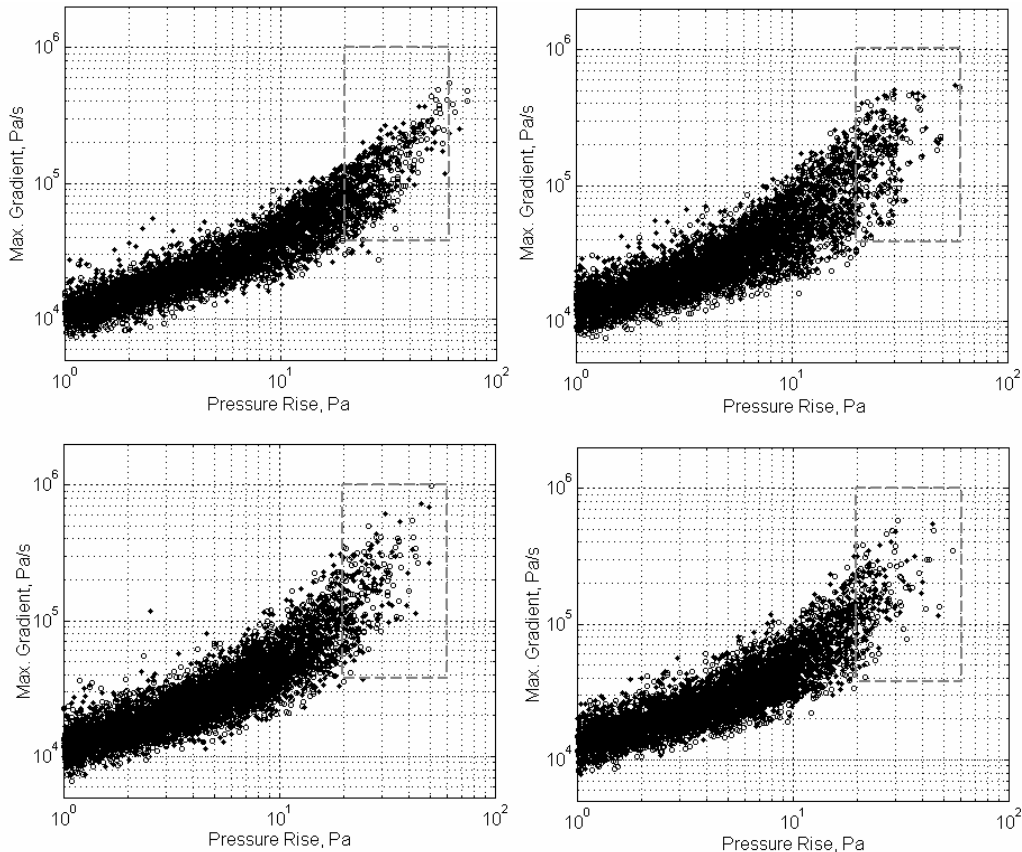


Figure 10. Pressure Rise versus Maximum Gradient Plots for Run 20. Clockwise from top left: ground, 5-ft, 13 and 26-ft, and 39-ft microphone results.

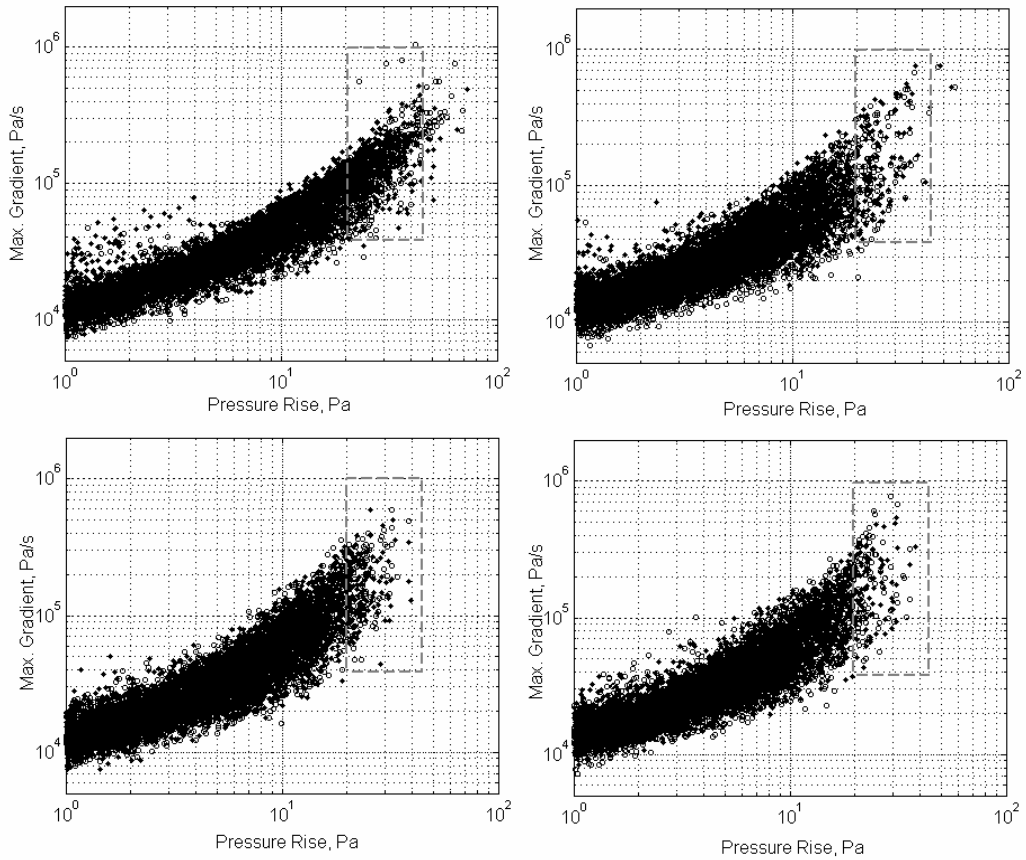
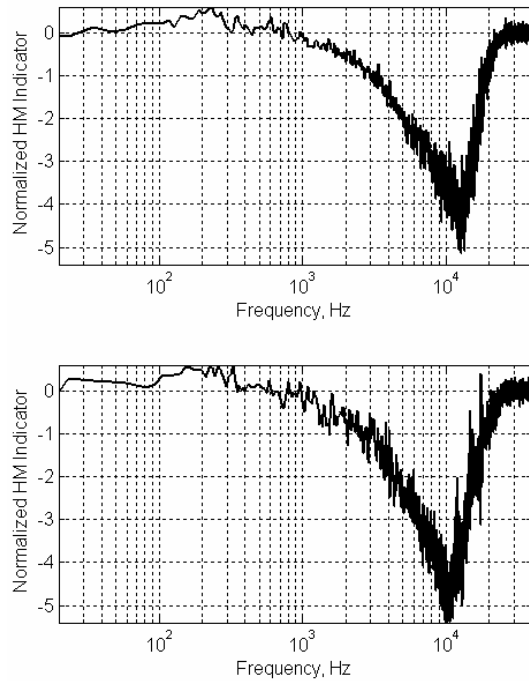


Figure 11. Pressure Rise versus Maximum Gradient Plots for Run 21. *Clockwise from top left: ground, 5-ft, 13 and 26-ft, and 39-ft microphone results.*

Figure 12. Normalized Howell Morfey Indicator calculated from data recorded by Microphone 4 at 39 feet during Run 20 (top) and Run 21.



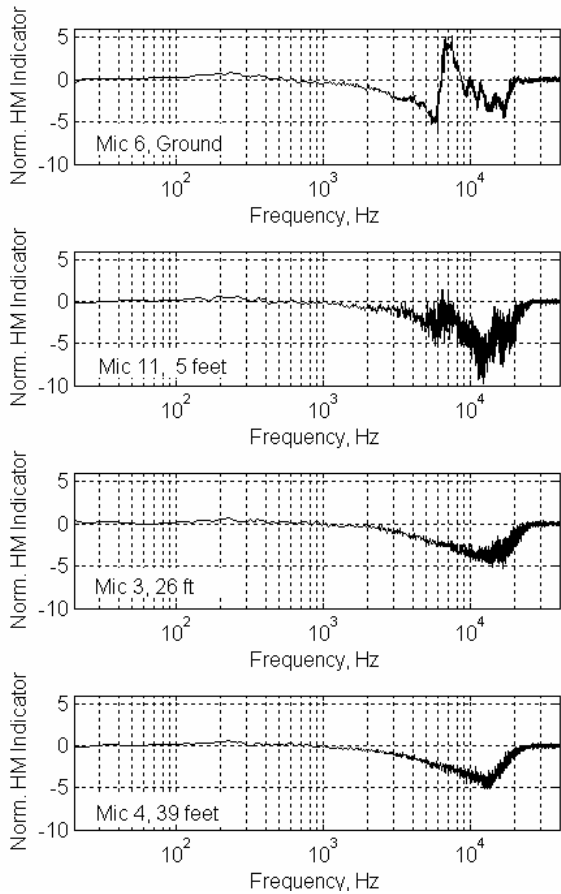


Figure 13. Variation of Normalized HM Indicator with Microphone Height. Data shown are Run 20, microphones 6 (top), 11, 3, and 4 (bottom).

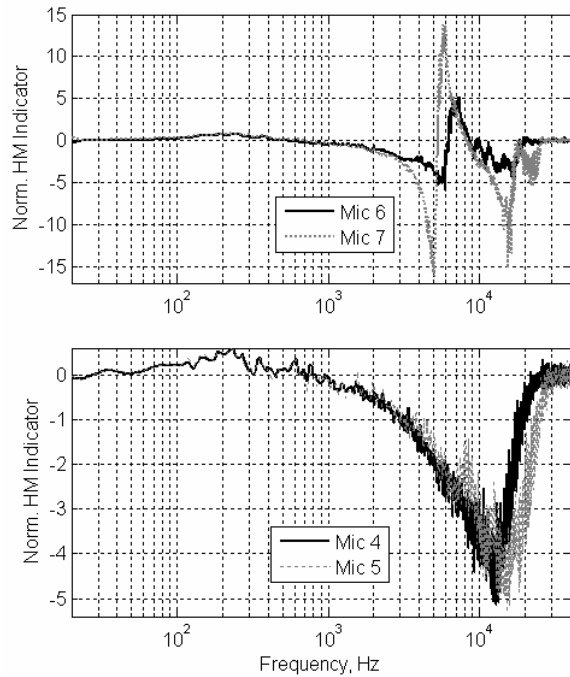


Figure 14. Run 20 Variation of Normalized HM Indicator for Different Microphones on the Ground (top) and at 39 feet (Bottom).

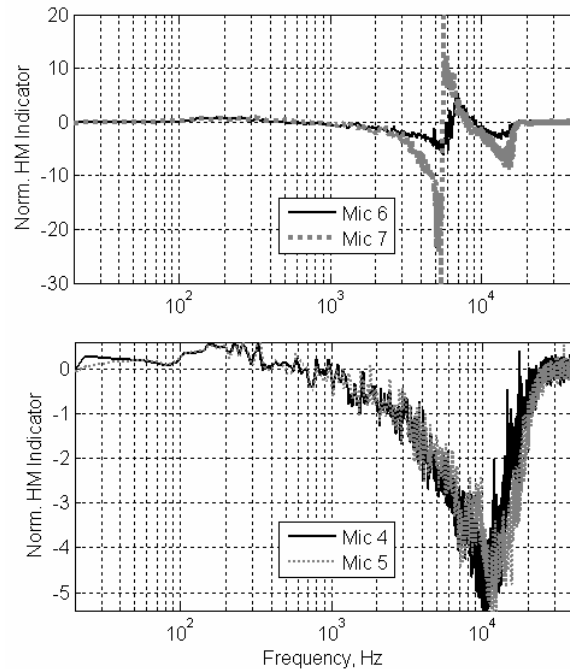


Figure 15. Run 21 Variation of Normalized HM Indicator for Different Microphones on the Ground (top) and at 39 feet (Bottom).